PLA Nanocomposites Reinforced with Cellulose Nanocrystals from *Posidonia oceanica* and ZnO Nanoparticles for Packaging Application

F. Luzi[1], E. Fortunati[1]*, A. Jiménez[2], D. Puglia[1], A. Chiralt[2] and L. Torre[1]

[1]*University of Perugia, Civil and Environmental Engineering Department, UdR INSTM, Strada di Pentima 4, 05100 Terni, Italy*
[2]*Institute of Food Engineering for Development, Polytechnic University of Valencia, Camino de Vera s/n, 46022 Valencia, Spain*

Received September 15, 2016; Accepted November 05, 2016

ABSTRACT: Poly(lactic acid) (PLA) based nanocomposites reinforced with 1 wt% of surfactant-modified cellulose nanocrystals (s-CNC) extracted from *Posidonia oceanica* plant waste and zinc oxide nanoparticles (ZnO NPs) at different concentrations (0.1 and 0.5 wt%) were prepared by solvent casting process. Their thermal, morphological, optical, mechanical and water vapor permeability properties were investigated. Tensile testing showed increased values for strength and deformation at break in PLA based formulations reinforced with s-CNC and ZnO NPs as a consequence of better nanofiller dispersion compared to binary films reinforced only with ZnO NPs. Moreover, the effect of s-CNC and ZnO NPs provoked an improvement of barrier properties, highlighting the synergic ability of nanofillers to increase the tortuous path of gas molecules, reducing the water vapor permeability coefficients, a property of fundamental importance in food packaging applications. Finally, antimicrobial activity was evaluated using two bacterial strains, *Escherichia coli* and *Listeria innocua*.

KEYWORDS: Nanocomposites, packaging, poly(lactic acid), cellulose nanocrystals, zinc oxide nanoparticles, plant waste, *Posidonia oceanica*

1 INTRODUCTION

In the last few decades, the need to extend the shelf life of packaged foods and the necessity to reduce their environmental impact has been of interest in academic research. The principal objective of food packaging applications is to extend shelf life and to maintain the quality and safety of food products during storage and distribution. Moreover, factors affecting flavors and aromas, such as the transmission of light, the movement of moisture, and the mass transfer of gases (O_2, CO_2, water vapor), usually occurring between the internal and external environment of the package, need to be controlled [1]. The estimation of the barrier properties of the polymeric materials is a critical characteristic useful in the prediction of product-package shelf life [2]. Moreover, the development of active and multifunctional features has good potential for improving the final characteristics of the package, such as the resistance to microbial growth. In fact, the use of antimicrobial agents or nanoparticles that come into contact with food can reduce or eliminate the growth of microorganisms in food products, reducing the deterioration of food products and improving their quality [3, 4].

In this context, increasing interest towards the environment has determined a rethinking of sustainable economic growth in a green framework. New biodegradable, eco-friendly and eco-sustainable materials extracted from natural sources for use in food packaging or in many short shelf-life applications represent a valid alternative to petroleum-based materials.

Poly(lactic acid) (PLA) is considered a valid alternative to petrochemical-based commodity plastics for reducing the carbon footprint and environmental impact [5]. It is an aliphatic thermoplastic crystalline polymer produced from natural resources by fermentation of polysaccharides or sugar [6]. Furthermore, PLA is approved by the US Food and Drug Administration (FDA) as a food contact substance and it is used as packaging material for some short shelf-life applications [7, 8]. The interest in PLA is due to its superior transparency, easy processability, and high mechanical properties with respect to other

*Corresponding author: elena.fortunati@unipg.it

DOI: 10.7569/JRM.2016.634135

green materials [9]. PLA possesses remarkable properties such as good biodegradability and biocompatibility [10, 11]. In addition to being an economically feasible material [12], it also has application in rigid and flexible food packaging [13] for the production of disposables, film packaging and bags [14]. The main limitations of PLA, and in general of biodegradable polymers, with respect to petroleum-based polymers, are related to its poor water vapor barrier properties (necessary for fresh food packaging), poor oxygen barrier characteristics and relatively limited thermal and mechanical properties [5, 15]. The need to extend the shelf life of packaged food has oriented research towards innovative solutions and, along with the changing needs of consumers, has made "packaging" a constantly evolving field [16–19].

In this context, the development of nanocomposite based formulations represents a valid method to improve the functional properties of biodegradable polymers, such as barrier, thermomechanical, antimicrobial and antifungal responses, without affecting their biocompatibility, transparency, and processability [20]. Recently, the use of different nanoscaled fillers has been proposed to modulate the final properties of biodegradable polymers, such as montmorillonite [21], sepiolite [22], carbon nanotubes [23], lignocellulosic nanostructures [24–27], and metal nanoparticles such as copper [28], silver [29] and ZnO [10, 30].

In this specific study, the combination of cellulose nanocrystals and commercial zinc oxide nanoparticles (ZnO NPs) in PLA matrix was investigated.

Cellulose nanocrystals (CNC) were used in PLA to improve the thermal, mechanical and gas barrier properties of the matrix. Cellulose can be obtained in the form of rigid rod monocrystalline domains with diameters ranging from 1–100 nm and from ten to hundreds of nm in length [31]; the nanocrystals' aspect ratio (diameter/length) can vary from 1:1 to 1:100 and they can have an elastic modulus of around 150 GPa [32].

Zinc oxide nanoparticles (ZnO NPs) are nontoxic and certificated as generally recognized as safe (GRAS) material [10]; they are well known as environmentally friendly and inorganic nanofiller for various polymers, providing properties like intensive ultraviolet absorption and antibacterial effect [33, 34]. In particular, ZnO particles at nanoscale level have more pronounced antimicrobial activities than large particles: the antibacterial activity of ZnO increases with decreasing particle size, moreover, high surface-to-volume ratio allows for a better interaction with bacteria [35]. They are used as food additive [36], in biomedical applications [37], and in catalysis [38]. ZnO nanoparticles have a wide range of antibacterial activities against both Gram-positive and Gram-negative bacteria [39, 40] and foodborne pathogens. The incorporation of ZnO nanoparticles into biodegradable polymers could improve not only mechanical and barrier properties, but also the antimicrobial activity of the polymeric matrix in which they are embedded [41].

The main objective of the present research was the validation of PLA based nanocomposite films reinforced with ZnO NPs (0.1 and 0.5 wt%) and surfactant-modified cellulose nanocrystals (s-CNC, 1 wt%) extracted from *Posidonia oceanica* ball wastes for possible use as potential packaging solutions. CNC modification, by means of a commercial surfactant, was applied in order to increase the dispersion of ZnO NPs in the PLA matrix [42] and the proposed formulations were produced by using a cheap solvent casting procedure.

Balls composed of the leaves of *Posidonia oceanica*, a sea grass plant in the Mediterranean Sea, sometimes accumulate on the coast, generating sea waste and causing several problems for the touristic coastal beaches [43]. In particular, the balls are characterized by relatively high amounts of extractives, especially ethanol/toluene extractives (10.7%), ash content (12%), and high cellulose content (40%) [44], which is the reason why the attention of the scientific community is oriented towards the revalorization of marine wastes for the preparation of high-tech composites or nanocomposite materials [45–47].

Revalorization of *Posidonia oceanica* as precursor for CNC extraction, already investigated in the literature [43, 44, 47], was reconsidered here with the aim of studying the combination of CNC with a metal nanoparticle in a multifunctional nanocomposite approach.

Both binary and ternary formulations, reinforced with ZnO NPs and/or s-CNC, were produced and their morphological, thermal, mechanical, optical and barrier properties were evaluated. In addition, a preliminary evaluation is presented of the antimicrobial and antifungal response of the produced films.

2 EXPERIMENTAL SECTION

2.1 Materials

Poly(lactic acid) (PLA) in the form of fibers was purchased from MiniFibers Inc. The polymer has a density of 1.25 g cm^{-3} and the length of the fibers is around 6 mm. *Posidonia oceanica* balls were collected from the Campello Beach in Alicante (Spain) by Aitex (Alcoy, Alicante, Spain) and used as raw material for the extraction of cellulose nanocrystals. The extraction of the cellulose nanocrystals (CNC) from *Posidonia oceanica* was previously described by Fortunati *et al*. and Luzi *et al*. [47, 48].

Zinc oxide powder was supplied by PlasmaChem GmbH (Average size: ca. 14 nm; Specific area: 30 ± 5 m^2g^{-1}; Purity: > 99%).

All the chemical reagents were supplied by Sigma-Aldrich and used as received.

2.2 Cellulose Nanocrystal Extraction and Characterization

The extraction of cellulose nanocrystals was performed in two steps (Figure 1). The first step consisted of a chemical treatment that permitted the obtainment of holocellulose by removing ash and lignin from the raw material, whereas the second process consisted of a sulphuric acid hydrolysis (64% [wt/wt] of sulphuric acid, at 45 °C for 30 minutes) which was able to remove the amorphous portion from cellulosic materials, obtaining CNC in an aqueous suspension.

The diameter of the unbleached raw fibers was investigated by means of field emission scanning electron microscopy (FESEM, Supra 25-Zeiss). The FESEM micrographs of both unbleached and bleached fibers were analyzed with NIS-Elements BR (Nikon) software for the determination of the distribution of fiber diameters. Sixty measurements were obtained as a representation of the diameter distribution. The unbleached fibers have a diameter of (84 ± 26) µm, while, after the chemical treatment, the fibers appeared bleached and more separated, characterized by a reduced diameter of about (7 ± 2) µm, as a consequence of the elimination of lignin and ashes. At the end of the chemical treatment, and after the acid hydrolysis, CNC appeared well individualized with the characteristic acicular rod shape. Length and diameter of cellulose nanocrystals were determined by using an atomic force microscope (AFM) from Digital Instruments having a NanoScope III controller with a MultiMode head (Veeco) and an integrated silicon tip/cantilever. The phase and height images were carried out working in a tapping mode.

CNC exhibit a length of (180 ± 28) nm and a diameter of (4.9 ± 1.3) nm with an aspect/ratio of 36.7 [47] (Figure 1) determined from a minimum of 80 measurements.

2.3 ZnO Nanoparticle Characterization

The morphology of zinc oxide nanoparticles was examined by field emission scanning electron microscopy (FESEM, Supra 25-Zeiss, Germany). ZnO nanoparticles were suspended in chloroform ($CHCl_3$) by vigorous stirring for 1 h followed by sonication (Vibracell, 750W) for 1 h at room temperature (RT); after that a few drops of the suspension were deposited onto a silicon substrate, dried at room temperature and finally analyzed.

2.4 PLA Nanocomposite Film Preparation

The PLA nanocomposite films were prepared by solvent casting method using the method described

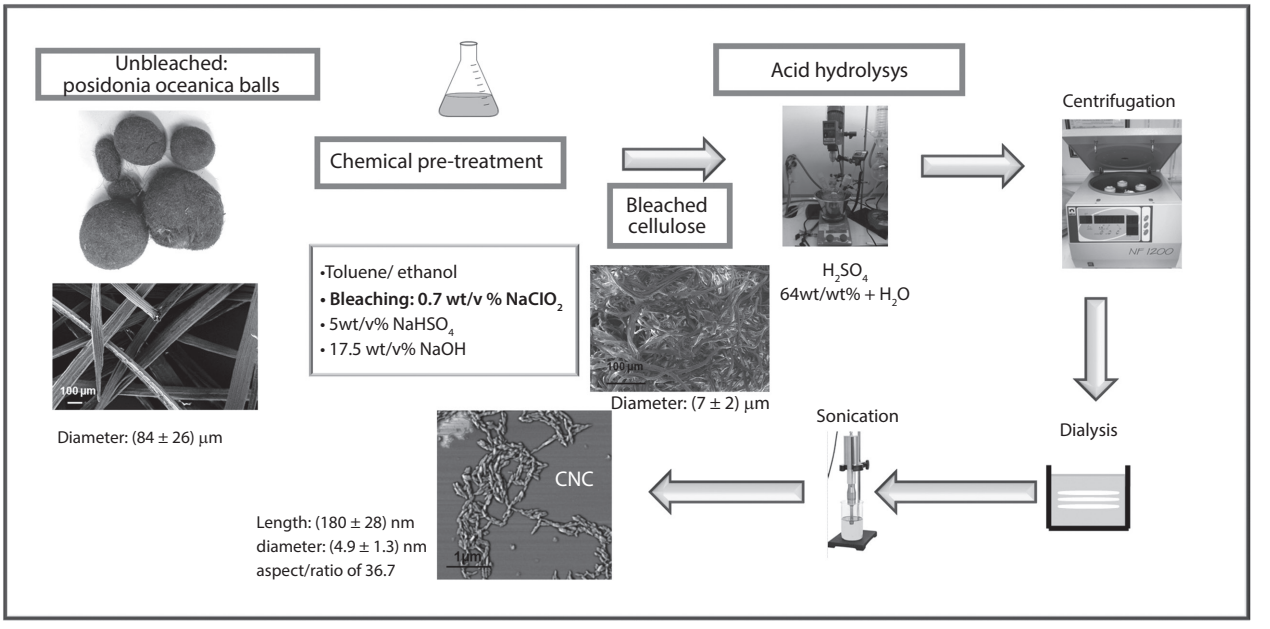

Figure 1 Scheme of CNC extraction and chemical and acid hydrolysis treatment.

 DOI: 10.7569/JRM.2016.634135

by Jayaramudu *et al.* [49] with minor modifications. Initially, PLA (1 g) was dissolved in 25 mL of $CHCl_3$ with stirring at RT. The solution was casted onto a 15 cm diameter Petri dish substrate covered with Teflon® and evaporated for 24 h at RT.

Binary PLA based nanocomposites reinforced with 1 wt% of surfactant-modified (s-CNC) cellulose nanocrystals were produced. The CNC were modified with a an acid phosphate ester of ethoxylatednonyl phenol, commercial surfactant (Beycostat A B09; CECCA S.A.) [50]. The solution of s-CNC was prepared adding the surfactant in the proportion of 1/4 (wt/wt) to the CNC aqueous suspension. In order to increase the thermal stability of the produced nanocrystals, pH of s-CNC solutions was raised approximately to 9, by using a 0.25 wt% NaOH solution [51]. After freeze-drying, chloroform was directly added to the cellulose powder, forming 1 wt% suspensions, and it was exposed to sonication (Vibracell, 750W) for 1 min in an ice bath. Subsequently, s-CNC suspension in chloroform was mixed with previously prepared PLA solution, casted on Petri dish as described above.

A similar procedure was used to produce binary PLA films loaded with ZnO NPs (PLA_ZnO): a predetermined amount (0.1 or 0.5 wt%) of ZnO NPs was dispersed in $CHCl_3$ by vigorous stirring for 1 h using magnetic stirrer at RT, followed by sonication (Vibracell, 750W) for 1 h at RT. The ZnO solution was mixed with the previously prepared PLA solution, sonicated for 30 min and casted onto a Petri dish substrate covered with Teflon.

Finally, PLA ternary films reinforced with ZnO NPs (0.1 or 0.5 wt%) and s-CNC (1 wt%) were produced: a specific amount of s-CNC previously dissolved in $CHCl_3$ was mixed with the solution of PLA and zinc oxide (PLA_ZnO described above) for 1 h under magnetic stirrer at RT.

Films with a thickness of approximately 50 µm were obtained for each formulation (Table 1).

Table 1 Material formulations.

Formulations	PLA	s-CNC (wt%)	ZnO (wt%)
PLA	100	–	–
PLA_1s-CNC	99	1	–
PLA_0.1ZnO	99.9	–	0.1
PLA_0.5ZnO	95.5	–	0.5
PLA_1s-CNC_0.1ZnO	98.9	1	0.1
PLA_1s-CNC_0.5ZnO	98.5	1	0.5

2.5 Characterization of PLA Nanocomposite Films

2.5.1 Morphological and Optical Properties

The microstructure of the PLA nanocomposite cryo-fractured surfaces was investigated by scanning electron microscope (FESEM, Supra 25-Zeiss, Germany) after a gold sputtering.

The transparency of the films was determined from the surface reflectance spectra obtained on white and black backgrounds from 400 to 700 nm, by using a spectrocolorimeter CM-3600d (Minolta Co., Tokyo, Japan) with a 30 mm diameter sample area by applying the Kubelka-Munk theory for multiple scattering to the reflection spectra. Internal transmittance (T_i) of the films was quantified using Equation 1. In this equation R_0 is the reflectance of the film on an ideal black background. Parameters *a* and *b* were calculated by Equations 2 and 3, where *R* is the reflectance of the sample layer backed by a white plate with known reflectance R_g. Six replicates were taken for each formulation.

$$T_i = \sqrt{(a - R_0)^2 - b^2} \tag{1}$$

$$a = \frac{1}{2}\left(R + \frac{R_0 - R + R_g}{R_0 R_g} \right) \tag{2}$$

$$b = \left(a^2 - 1\right) \tag{3}$$

Gloss was measured using a flat surface gloss meter (Multi-Gloss 268, Minolta, Langenhagen, Germany) at an incidence angle of 60°, according to the ASTM standard D523 [52]. The measurements were performed over a black matte standard plate and six measurements were taken for each formulation. The data were expressed as gloss units, relative to a highly polished surface of standard black glass with a gloss value close to 100.

2.5.2 Thermal and Mechanical Properties

The thermal stability of the samples was determined by means of thermogravimetric analysis (TGA) using a Seiko Exstar 6300. A heating scan from 30 to 600 °C at 10 °C min^{-1} in nitrogen atmosphere (250 mL min^{-1}) was performed for each sample.

Differential scanning calorimeter (DSC) measurements were performed by using a Mettler Toledo 822/e DSC under nitrogen atmosphere; two heating and one cooling scans were carried out in the temperature range from –25 to 210 °C, at 10 °C min^{-1}. Melting and cold crystallization temperatures and enthalpies (T_m, T_{cc} and ΔH_m, ΔH_{cc}) were determined from the first

and second heating scan, while crystallization phenomena were detected from the cooling scan. The glass transition temperature (T_g) was registered from each scan. Three samples were used to characterize each formulation.

The crystallinity degree was calculated by using Equation 4:

$$\chi = \frac{1}{\left(1-m_f\right)}\left[\frac{\left(\Delta H_m - \Delta H_{cc}\right)}{\Delta H_0}\right]\times 100 \qquad (4)$$

where ΔH_m is the melt enthalpy and ΔH_{cc} is the cold crystallization enthalpy, ΔH_0 is enthalpy of melting for a 100% crystalline PLA sample, taken as 93 J g^{-1} [53]), m_f is the weight fraction of nanoreinforcements in the sample and $(1–m_f)$ is the weight fraction of PLA in the sample.

The mechanical properties of neat PLA and PLA nanocomposites were evaluated by tensile tests, performed on rectangular samples (50 × 10 mm^2) on the basis of UNI ISO 527, with a load cell of 500 N, a crosshead speed of 1 mm min^{-1} and an initial gauge length of 25 mm.

Average tensile strength (σ_b), elongation at break (ε_b), and Young's modulus (E) were calculated from the resulting stress-strain curves. The specimens were dried in a vacuum oven at 40 °C for 72 h, then cooled in a desiccator and immediately tested. The measurements were done at RT and at least five samples for each formulation were tested.

2.5.3 Barrier Properties

Water vapor permeability (WVP) of PLA and PLA nanocomposites was evaluated by using Payne permeability cups (Payne, elcometer SPRL, Hermelle/sd Argenteau, Belgium) of 3.5 cm diameter, according to the ASTM E96-95 gravimetric method [54]. Deionized water or lithium chloride oversaturated solutions were used inside the testing cups to achieve, respectively, 11 or 100% RH on one side of the film; meanwhile, an oversaturated magnesium nitrate-6-hydrate solution was used to control the RH (53% RH) on the other side of the film. The relative humidity gradient (53–100% or 11–53%) of the tests was selected according to the final use of the flexible films as packaging material, thus simulating the contact with fresh food (meat or fresh cut fruit) or very low water activity products. A fan placed on the top of the cup was used to reduce resistance to water vapor transport. Water vapor transmission rate (WVTR) measurements were performed at 25 °C.

The cup weights were taken every 2 h using an analytical balance (±0.00001 g).

For the calculation of WVTR, slopes in the steady-state period of the weight loss vs. time curves were determined by linear regression, once normalized to the film areas.

Four WVP measurements were taken for each type of film.

2.5.4 Antimicrobial Assays

The evaluation of the antibacterial activity of PLA nanocomposite films was done by a turbidity method by using a UV-Vis spectrometer (Thermo Scientific Evolution 201) with two strains of bacteria such as *Escherichia coli* (Gram negative) and *Listeria innocua* (Gram positive).

Stock culture of *E. coli* and *L. innocua* (CECT), supplied by the Spanish Type Culture Collection (CECT, Burjassot, Spain), was kept frozen (–25 °C) in Tryptone Soy Broth (TSB, Scharlab, Barcelona, Spain) supplemented with 30% glycerol (Panreac Química, Castellar del Vallés, Barcelona, Spain). The culture was regenerated by transferring a loopful of bacteria into 10 mL of TSB; the tubing was incubated at 37 °C overnight. Subsequently, 10 µL aliquot of bacterial solution was transferred into 10 mL of potato dextrose broth and grown at 37 °C for 24 h to reach the exponential phase of growth. Under sterile conditions, aliquots of potato dextrose broth (10 mL) were poured into tubing and inoculated with 10 µL of bacterial solution. This culture, appropriately diluted, was then used for inoculation of the agar plates in order to obtain a target inoculum of approximately 10^2 CFU/cm^{-2}. Films of 1 × 2 cm^2 (containing or not ZnO nanoparticles) were placed into tubing and stored for 1 day at 37 °C. Cell survival was expressed as the number of colony-forming unit (CFU) of bacteria growth. Tubes without film and the tubes with only 0.5 wt% of ZnO nanoparticles with respect to the estimated weight of films were also incubated as controls. The absorbance of different tubes was measured at 550 nm and correlated with the total microbial count. Previous to testing, a calibration curve was obtained by using different dilutions from the culture on exponential phase of growth whose absorbance was properly measured.

2.6 Statistical Analysis

Results were analyzed by analysis of variance (ANOVA) using the Statgraphics Plus 5.1 program (Manugistics, Inc., Rockville, MD). To differentiate samples, Fisher's least significant difference (LSD) was used at the 95% confidence level.

 DOI: 10.7569/JRM.2016.634135

3 RESULTS AND DISCUSSION

3.1 ZnO Nanoparticles: Morphological Characterization and Processing Optimization

Figure 2 shows the FESEM images of commercial zinc oxide nanoparticles. Specifically, Figure 2a shows the microstructures of ZnO NPs in powder, while Figure 2b shows the morphological investigation of NPs after the suspension in chloroform. The presence of different agglomerates was observed in the commercial ZnO NPs powder (Figure 2a): in order to reduce this problem, magnetic stirring and sonication procedures were applied according to Jayaramudu *et al*. [49] to enhance their dispersion. The treatment permitted to obtain individualized NPs with nanometric dimension (Figure 2b). Sonication in addition to magnetic stirring was considered as a valid strategy of fundamental importance to improve the NPs dispersion into $CHCl_3$ solution.

3.2 PLA Nanocomposite Characterization

3.2.1 Morphological and Optical Properties

In order to evaluate the influence of surfactant-modified cellulose nanocrystal and ZnO nanoparticles on the cross-section morphology of PLA matrix, fractured surfaces of PLA based nanocomposites (Figure 3) were investigated by FESEM. A relatively smooth fractured surface was observed for the neat PLA film [47, 49], whereas a porous structure induced by the presence of the surfactant-modified s-CNC was detected. PLA_1s-CNC fractured surface showed great evidence of the uniform dispersion of modified cellulose nanocrystals and plastic deformation [26]. The presence of ZnO nanoparticles in the binary systems did not affect the PLA cross-section structure, confirming the homogeneous dispersion of metallic nanoparticles [55]. A similar behavior was detected for the PLA_s-CNC_ZnO based systems. Ternary systems showed a more compact topography, especially when the highest content of ZnO was added. The presence of s-CNC enhanced distribution of ZnO nanoparticles (see cross-section PLA_1s-CNC_0.1ZnO and PLA_1s-CNC_0.5ZnO), reducing the porous structure of the cross section.

Table 2 shows the values of the internal transmittance (T_i) at 450 nm and the gloss values at 60° for PLA and PLA nanocomposites. The gloss and transparency of the films are relevant properties for packaging applications. High values of T_i are associated with transparent films with structural homogeneity and their degree of transparency according to Kubelka-Munk theory. The highest T_i value was found for neat PLA and no significant changes ($p < 0.05$) were detected for all the produced PLA based nanocomposites despite the microstructural differences observed by FESEM. The particle size was small enough to not significantly alter

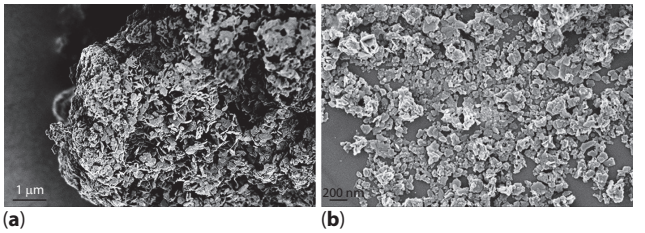

Figure 2 FESEM investigation of ZnO NPs in powder (**a**) and after the suspension in chloroform (**b**).

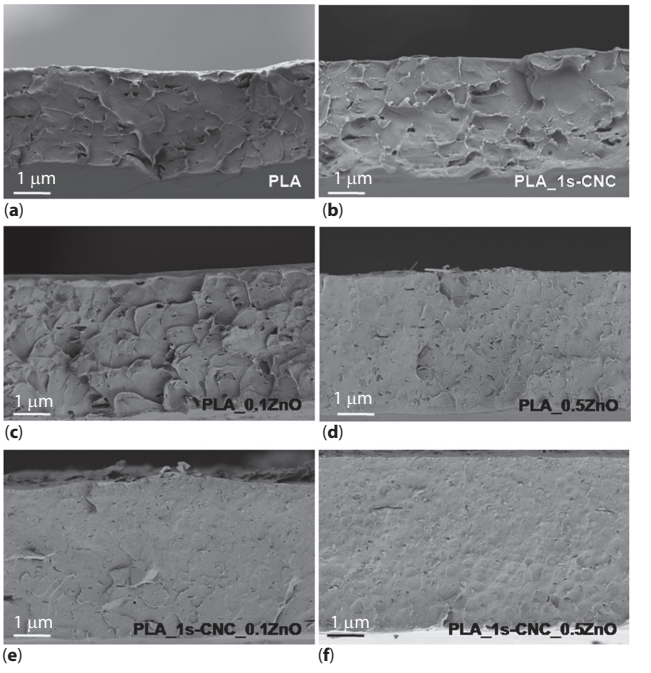

Figure 3 FESEM investigation of the fractured surfaces of PLA and PLA nanocomposites.

Table 2 Internal transmittance at 450 nm and gloss at 60 ° values for PLA and PLA nanocomposites.

Formulations	Ti (450 nm)	Gloss 60 °
PLA	87.8 ± 0.2^{c}	36.1 ± 2.4^{ab}
PLA_1s-CNC	87.3 ± 0.1^{b}	42.8 ± 0.7^{d}
PLA_0.1ZnO	87.5 ± 0.3^{bc}	36.1 ± 2.1^{ab}
PLA_0.5ZnO	87.3 ± 0.2^{b}	34.7 ± 2.5^{a}
PLA_1s-CNC_0.1ZnO	87.2 ± 0.2^{a}	39.7 ± 1.8^{c}
PLA_1s-CNC_0.5ZnO	86.6 ± 0.2^{a}	38.6 ± 1.2^{bc}

Different letter in the same column indicate significant differences among formulations ($p<0.05$).

the light dispersion pattern in the film in the range of visible radiation. On the other hand, the gloss values for PLA nanocomposites were affected by the presence of both ZnO nanoparticles and/or surfactant-modified cellulose nanocrystals. In the case of binary nanocomposites reinforced with ZnO nanoparticles (PLA_ZnO), the gloss values slightly decreased at the highest filler percentage content, whereas no significant differences with respect to neat PLA were observed for the lowest ratio. However, an increase in gloss values was observed for films reinforced with 1 wt% of s-CNC, both in binary (PLA_1s-CNC) and ternary nanocomposites (PLA_1s-CNC_ZnO) (Table 2). The increase of gloss values induced by the presence of cellulosic fillers could be ascribed to their optical and chiral properties [56, 57]. Moreover, this effect can be related to the good distribution of s-CNC in PLA matrix during the process [26]. Finally, this effect was also evident and maintained for the ternary based systems, especially in the case of PLA_1s-CNC_0.1ZnO film.

3.2.2 Thermal Properties

The effect of ZnO nanoparticles and s-CNC on the thermal properties of the PLA matrix was investigated by thermogravimetric (TGA) measurements and differential scanning calorimeter (DSC). Specifically, the derivative curves of the mass loss (DTG) are reported in Figure 4a, while the curves and the data from the second heating scan of the DSC measurements are reported in Figure 4b and Table 3, respectively.

The PLA decomposed in a single-step process (Figure 4a) with an initial degradation temperature (T_{onset}) of 270 °C and a temperature of maximum degradation rate (T_{max}) centered at 332 °C. The s-CNC based nanocomposites showed a similar behavior with respect to the PLA neat film. The temperatures of maximum degradation rate were observed at 330 °C, 309 °C, 292 °C, 331 °C and 305 °C for PLA_1s-CNC, PLA_0.1ZnO, PLA_0.5ZnO, PLA_1s-CNC_0.1ZnO and PLA_1s-CNC_0.5ZnO, respectively. The data revealed that the PLA_1s-CNC based system showed

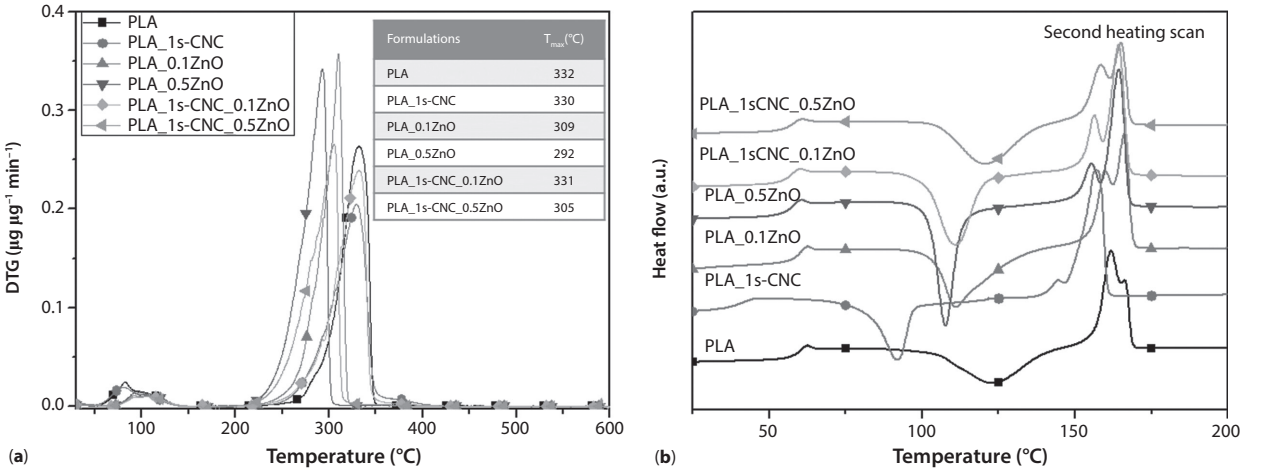

Figure 4 Derivative curves of the mass loss (DTG) (**a**) and DSC thermograms at the second heating scan (**b**) of PLA and PLA nanocomposites.

Table 3 Thermal properties from DSC measurements of PLA and PLA nanocomposites.

Formulations	Second heating scan						
	T_g (°C)	ΔH_{cc} (Jg^{-1})	T_{cc} (°C)	ΔH_m (Jg^{-1})	T'_m (°C)	T''_m (°C)	χ (%)
PLA	56.2 ± 0.8^{b}	31.2 ± 4.0^{b}	118.6 ± 4.8^{c}	37.4 ± 3.9^{a}	161.1 ± 2.1^{f}	163.1 ± 2.1^{b}	5.2 ± 1.0^{b}
PLA_1s-CNC	40.6 ± 0.3^{a}	22.0 ± 3.5^{a}	91.5 ± 0.5^{a}	39.3 ± 2.8^{a}	144.7 ± 0.2^{a}	157.2 ± 0.2^{a}	18.5 ± 0.7^{c}
PLA_0.1ZnO	60.3 ± 0.5^{d}	36.1 ± 1.2^{b}	111.4 ± 0.6^{b}	38.7 ± 0.3^{a}	159.8 ± 0.4^{e}	166.9 ± 0.1^{c}	4.1 ± 0.6^{a}
PLA_0.5ZnO	57.5 ± 0.7^{bc}	36.1 ± 0.6^{b}	107.5 ± 0.2^{b}	38.74 ± 0.3^{a}	155.3 ± 0.3^{b}	164.3 ± 0.1^{bc}	2.7 ± 0.4^{a}
PLA_1s-CNC_0.1ZnO	57.9 ± 0.1^{c}	36.6 ± 0.4^{b}	111.0 ± 0.2^{b}	38.7 ± 0.5^{a}	156.5 ± 0.4^{c}	164.4 ± 0.2^{bc}	2.9 ± 0.2^{a}
PLA_1s-CNC_0.5ZnO	57.7 ± 1.1^{bc}	32.9 ± 1.1^{b}	110.6 ± 0.1^{c}	35.7 ± 0.8^{a}	157.9 ± 0.2^{d}	164.9 ± 0.2^{bc}	3.0 ± 0.3^{a}

Different letter in the same column indicate significant differences among formulations ($p < 0.05$).

the highest thermal stability (main peak at 330 °C), whereas the presence of ZnO conductive nanoparticles induced a shift of the PLA maximum degradation rate temperature to lower temperatures [55], as already observed in the presence of metal particles [58, 59]. This effect was more evident for the highest content of ZnO NPs (0.5 wt%). In this context, the work of Murariu *et al.* [55] confirms that the reduction in thermal stability can be directly correlated with the content of ZnO NPs. Moreover, this effect could also be related to the catalytic role of zinc products produced at high temperature in the promotion and selective formation of lactide and related oligomers during PLA degradation [55, 60]. On the basis of these considerations, the lowest values of maximum degradation rate temperatures detected for the binary formulations were justified, specifically for PLA_0.5ZnO. On the other hand, the combination of s-CNC and ZnO NPs in ternary films was able to induce slightly higher thermal stability. This behavior was already observed by Ahmed *et al.* in PLA matrix modified with ZnO nanoparticles and polyethylene glycol [61], where the presence of additives disturbed the gas release from decomposed samples and delayed the mass loss.

The DSC thermal properties of the second heating scan are summarized in Table 3 and the curves are shown in Figure 4b. During the second heating scan, significant changes ($p < 0.05$) were observed in the glass transition temperature (T_g) of PLA_ZnO based films with respect to the neat PLA (56.2 ± 0.8) °C [55].

The presence of ZnO nanoparticles increased the rigidity of the systems and consequently an increase in glass transition temperatures was measured. On the contrary, PLA_1s-CNC showed a significant shift (about 15 °C) to lower T_g values with respect to PLA film [47]. This phenomenon could be ascribed to the presence of surfactant that induced a plasticizer effect, confirmed by FESEM investigation, in which a less brittle fractured surface for PLA nanocomposites reinforced with s-CNC was observed. PLA and PLA based nanocomposites were characterized by a marked exothermic cold crystallization phenomenon with no significant differences induced by the presence of CNC or ZnO or their combination, confirming the amorphous or low crystalline nature of the studied formulations, as reported by Pantani *et al.* [18]. The endothermic or melting enthalpy (ΔH_m) remained the same with no particular changes ($p < 0.05$) for the different nanocomposites [18]. A reduction in the cold crystallization temperatures (T_{cc}) was observed for PLA_1s-CNC- and PLA_ZnO based nanocomposites, with a more visible effect in the case of PLA_1s-CNC, which showed a significant ($p < 0.05$) shift to lower temperatures of about 27 °C with respect to PLA: this behavior could be attributed to the nucleation effect of s-CNC in PLA matrix [47]. This effect was reduced in the case of PLA_1s-CNC_ZnO film: the presence of ZnO nanoparticles could reduce the nucleating effect of surfactant-modified cellulose nanocrystals. The double melting peak temperatures (T_m) for all produced films could be attributed to the melting of small and imperfect crystals formed during the cooling scan that change into more stable crystals through melting and recrystallization at low heating rates [62, 63].

3.2.3 Mechanical Response

Mechanical parameters of PLA and PLA nanocomposites, evaluated from stress-strain curves obtained performing tensile tests at RT, are summarized in Table 4. The addition of ZnO nanoparticles in binary formulations (PLA_ZnO) provoked a clear reduction of the elongation at break [18, 49, 55], and, at the same time, an increase in the strength at break, highlighting a brittle nature induced in the PLA matrix by the presence of the ZnO nanoparticles. The addition of surfactant modified cellulose nanocrystals into the PLA_ZnO based systems was able to modulate the mechanical response of the ternary formulations, with an increase in the elongation at break values when compared with PLA_ZnO binary films. This effect was particularly evident for the PLA_0.1ZnO_1s-CNC based system. The good dispersion of cellulose nanocrystals in PLA matrix could be due to the ability of the surfactant to cover the nanocellulosic reinforcements, increasing the interaction of nanofiller with polymer matrix [55]. Moreover, no particular changes ($p < 0.05$) were registered for the Young's modulus for all the produced PLA based nanocomposites.

Furthermore, a positive effect on the PLA mechanical response was induced by s-CNC addition with a relevant increase in tensile strength and a slight increase in the elongation at break [47]. This positive effect of cellulosic nanostructures was also confirmed in the ternary films and especially for the

Table 4 Mechanical properties of PLA and PLA nanocomposite.

Formulations	σ_b (MPa)	ε_b (MPa)	E_{Young} (MPa)
PLA	16.5 ± 3.1^{a}	277 ± 33^{cd}	1205 ± 100^{a}
PLA_1s-CNC	22.9 ± 1.2^{b}	286 ± 25^{d}	993 ± 190^{a}
PLA_0.1ZnO	20.5 ± 2^{b}	105 ± 10^{a}	1163 ± 33^{a}
PLA_0.5ZnO	38.3 ± 3.6^{c}	87 ± 8^{a}	1210 ± 50^{a}
PLA_1s-CNC_0.1ZnO	21.7 ± 1.6^{b}	250 ± 45^{bc}	975 ± 60^{a}
PLA_1s-CNC_0.5ZnO	23.7 ± 0.8^{b}	205 ± 15^{b}	990 ± 40^{a}

Different letter in the same column indicate significant differences among formulations ($p < 0.05$).

PLA_1s-CNC_0.1ZnO system that showed a relevant improvement in the elongation at break (ε_b) value with respect to PLA_0.1ZnO binary film, as a consequence of the synergic effect of s-CNC and ZnO particles and their better dispersion into PLA (as observed by FESEM investigation; see Figure 3). Concluding, the synergic combination of s-CNC and ZnO nanoparticles improved the mechanical response, in particular for PLA_1s-CNC_ZnO film, which appeared to be the ideal formulation in terms of mechanical performance required in food and in general for packaging applications.

3.2.4 Barrier Properties: Water Vapor Permeability

The evaluation of water vapor barrier properties is one of the most important requirements for food packaging, so the control of the moisture of food contained in the packaging are of relevant importance. The principal objective of food packaging is not only to contain and preserve food during the transport and storage, but also to reduce external contaminations, increasing its shelf life [64]. Furthermore, the determination of water vapor permeability behavior represents an important property to be determined, since it has a great effect on microbial growth and influences the shelf life of the packed products [65, 66].

Table 5 summarizes the water vapor permeability (WVP) coefficients for PLA and PLA binary and ternary nanocomposites.

All values obtained at 53–100% RH gradient were higher than those obtained at 11–53% RH gradient, which indicates that the film structure was slightly plasticized by the moisture content when it is in contact with high RH, despite the low water sensitivity of PLA.

The incorporation of nanoparticles significantly reduced the WVP of PLA films, depending on the type and concentration as well as the RH gradient used in the measurement. In general, the reduction percentage with respect to the net PLA films was slightly higher at 53–100% RH gradient (Table 5). The efficiency of ZnO nanoparticles at reducing WVP increased with their increase in concentration in the film. Likewise, in ternary composites, additive contributions of ZnO and CNC could be observed in terms of WVP reduction with respect to PLA films. A similar positive effect on the enhancement of the water barrier properties was also observed in the literature combining ZnO NPs with a biodegradable polymer [18]. A more evident effect in the water vapor barrier properties was detected in the ternary formulations produced combining s-CNC and ZnO nanoparticles in PLA matrix. A reduction of 14–20% was detected in the case of ternary systems PLA_1s-CNC_0.1ZnO and PLA_1s-CNC_0.5ZnO respectively in the case of 11–53% RH, while a reduction of 16–22% for the same formulations was observed in the case of 100–53% RH with respect to PLA film. The reduction of WVP values for nanocomposites with respect to PLA film can probably be ascribed to the homogeneous distribution of different nanofillers into PLA based formulations, as confirmed by FESEM investigations (see Figure 3). The presence of nanofiller increased the tortuous path of gas molecules through the nanocomposite structure and consequently an improvement of the barrier properties was observed [65, 67].

3.2.5 Antimicrobial Activity

Figure 5a,b shows the results of the antimicrobial activity evaluated using a turbidity test method for *Escherichia coli* and *Listeria innocua*, respectively. No inhibition of the bacterial growth was observed using *E. coli* and *L. innocua* and there were no significant changes ($p < 0.05$) detected for all the produced PLA based nanocomposites with regard to both bacteria.

The negative results could be attributed to the limited diffusion of ZnO nanoparticles to the aqueous culture

Table 5 Water vapour permeability coefficients for PLA and PLA nanocomposites.

Formulations	WVP (11–53% RH)		WVP (100–53% RH)	
	WVP (g mm/kPa h m²)	% Reduction	WVP (g mm/kPa h m²)	% Reduction
PLA	0.051 ± 0.004^{d}	–	0.067 ± 0.006^{c}	–
PLA_1s-CNC	0.047 ± 0.002^{bc}	8	0.059 ± 0.002^{ab}	12
PLA_0.1ZnO	0.048 ± 0.005^{bc}	6	0.063 ± 0.007^{bc}	6
PLA_0.5ZnO	0.046 ± 0.003^{bc}	10	0.058 ± 0.002^{ab}	13
PLA_1s-CNC_0.1ZnO	0.044 ± 0.001^{ab}	14	0.056 ± 0.001^{a}	16
PLA_1s-CNC_0.5ZnO	0.041 ± 0.002^{a}	20	0.052 ± 0.005^{a}	22

Different letter in the same column indicate significant differences among formulations ($p < 0.05$).

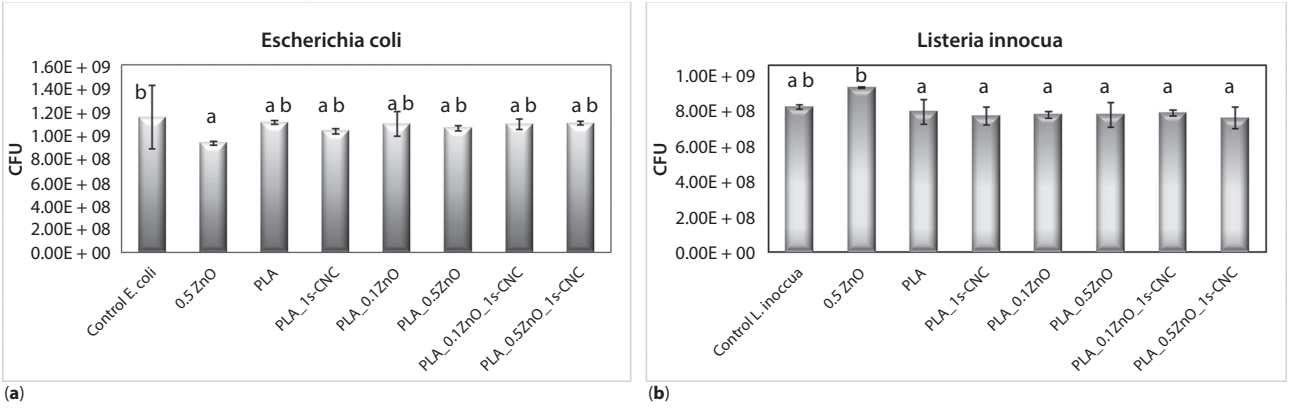

Figure 5 Antimicrobial activity of PLA and PLA nanocomposites against *Escherichia coli* (**a**) and *Listeria innocua* (**b**).

media, given the hydrophobic nature of the polymer matrix, which does not permit reaching the minimal inhibitory concentration (MIC) of the active in order to be effective against the tested bacteria. Higher ZnO concentrations in the film could enhance the compound release, thus promoting the antimicrobial action. Pantani *et al.* [18] observed that a low concentration of ZnO nanoparticles inferior to 1 and 3 wt% with respect to PLA is not able to reduce the bacterial growth of *Escherichia coli* and *Staphylococcus aureus*, respectively.

The mechanisms responsible for the antibacterial activity of ZnO nanoparticles are not very clear [68], however, it is thought that the antimicrobial effect can be mainly ascribed to the photocatalytic generation of a large number of reactive oxygen species (generation of hydrogen peroxide, superoxide anions and hydroxyl radicals), to the capture of ZnO onto the cell membrane [18, 30, 69] and formation of Zn^{2+} ions [70]. As mentioned above, the lack of antimicrobial activity of ZnO NPs in the hydrophobic film of PLA can be explained by the low diffusion of the zinc ions through the matrix which, in turn, exhibit low water sensitivity. This statement is supported by the fact that Shalumon *et al.* indeed observed antimicrobial activity (with two different bacterial strains, *Staphylococcus aureus* and *Escherichia coli*) even by using a low concentration (0.5 wt%) of ZnO NPs in a poly(vinyl alcohol) (PVA) hydrophilic matrix [41]. In fact, PVA favors the swelling phenomenon, facilitating the release of Zn^{2+} ions into the aqueous media where the microorganisms are present.

4 CONCLUSIONS

Poly(lactic acid) based nanocomposite films reinforced with 1 wt% of surfactant-modified cellulose nanocrystals extracted from *Posidonia oceanica* and commercial ZnO nanoparticles (0.1 and 0.5 wt%) were successfully produced by a solvent casting method. All the nanocomposites maintained the optical transparency of the PLA matrix, while morphological investigations underlined a rougher fractured surface for PLA_ZnO based systems and a more porous structure induced by the presence of surfactant-modified nanocellulose s-CNC. Data from mechanical tests confirmed the plasticization effect induced by s-CNC, suggesting the possibility of modulating mechanical properties according to application requests. The stress at break increases, while the elongation at break decreases with an increasing amount of ZnO nanoparticles in PLA matrix; in addition, a positive effect in terms of elongation at break was observed by combining s-CNC with ZnO NPs in PLA matrix. The combination of both nanoscaled reinforcements was able to increase the tortuous path of water vapor molecules, improving the WVP of the PLA matrix. Finally, no antimicrobial activity was observed by using low content of ZnO nanoparticles.

In conclusion, it is possible to note that PLA_1s-CNC_0.1ZnO film represents an interesting compromise for the modulation of functional properties of packaging application, suggesting the possibility of producing high-performance nanocomposites with remarkable properties by considering revalorized biomass wastes in combination with nanoparticles already widely studied and approved as antimicrobial agent in the food packaging sector.

Acknowledgments

The authors acknowledge the financial support of SEAMATTER: Revalorization of coastal algae wastes in textile nonwoven industry with applications in building noise isolation, LIFE11 ENV/E/000600, Funding Program: LIFE+. Call 2011.

References

1. J.W. Rhim, Effect of PLA lamination on performance characteristics of agar/κ-carrageenan/clay bio-nanocomposite film. *Food Res. Int.* **51**, 714–722 (2013).
2. V. Siracusa, P. Rocculi, S. Romani, and M. Dalla Rosa, Biodegradable polymers for food packaging: A review. *Trends Food Sci. Tech.* **19**, 634–643 (2008).
3. M. Alboofetileh, M. Rezaei, H. Hosseini, and M. Abdollahi, Antimicrobial activity of alginate/clay nanocomposite films enriched with essential oils against three common foodborne pathogens. *Food Control* **36**, 1–7 (2014).
4. G. Gorrasi, V. Bugatti, and V. Vittoria, Pectins filled with LDH-antimicrobial molecules: Preparation, characterization and physical properties. *Carbohyd. Polym.* **89**, 132–137 (2012).
5. M.P. Arrieta, M.M. Castro-López, E. Rayón, L.F. Barral-Losada, J.M. López-Vilariño, J. López, M.V. González-Rodríguez, Plasticized poly(lactic acid)–poly(hydroxybutyrate) (PLA–PHB) blends incorporated with catechin intended for active food-packaging applications. *J. Agric. Food. Chem.* **62**, 10170–10180 (2014).
6. R.M. Rasal, A.V. Janorkar, and D.E. Hirt, Poly(lactic acid) modifications. *Prog. Polym. Sci.* **35**, 338–356 (2010).
7. M.P. Arrieta, J. López, S. Ferrándiz, and M.A. Peltzer, Characterization of PLA-limonene blends for food packaging applications. *Polym. Test.* **32**, 760–768 (2013).
8. S.W. Hwang, J.K. Shim, S.E.M. Selke, H. Soto-Valdez, L. Matuana, M. Rubino, and R. Auras, Poly(L-lactic acid) with added α-tocopherol and resveratrol: Optical, physical, thermal and mechanical properties. *Polym. Int.* **61**, 418–425 (2012).
9. M.P. Arrieta, J. López, A. Hernández, and E. Rayón, Ternary PLA–PHB–Limonene blends intended for biodegradable food packaging applications. *Eur. Polym. J.* **50**, 255–270 (2014).
10. R.T. De Silva, P. Pasbakhsh, S.M. Lee, and A.Y. Kit, ZnO deposited/encapsulated halloysite–poly (lactic acid) (PLA) nanocomposites for high performance packaging films with improved mechanical and antimicrobial properties. *Appl. Clay Sci.* **111**, 10–20 (2015).
11. P. Chaiwutthinan, V. Pimpan, S. Chuayjuljit, and T. Leejarkpai, Biodegradable plastics prepared from poly(lactic acid), poly(butylene succinate) and microcrystalline cellulose extracted from waste-cotton fabric with a chain extender. *J. Polym. Environ.* **23**, 114–125 (2015).
12. R. Auras, B. Harte, and S. Selke, An overview of polylactides as packaging materials. *Macromol. Biosci.* **4**, 835–864 (2004).
13. D. Boonyawan, S. Sarapirom, S. Tunma, C. Chaiwong, P. Rachtanapun, and R. Auras, Characterization and antimicrobial properties of fluorine-rich carbon films deposited on poly(lactic acid). *Surf. Coat Technol.* **205**(Suppl. 2), S552–S557 (2011).
14. R.A. Auras, S.P. Singh, and J.J. Singh, Evaluation of oriented poly (lactide) polymers vs. existing PET and oriented PS for fresh food service containers. *Packag. Technol. Sci.* **18**, 207–216 (2005).
15. L. Petersson, I. Kvien, and K. Oksman, Structure and thermal properties of poly(lactic acid)/cellulose whiskers nanocomposite materials. *Compos. Sci. .Technol.* **67**, 2535–2544 (2007).
16. S. Burt, Essential oils: Their antibacterial properties and potential applications in foods—A review. *Int. J. Food Microbiol.* **94**, 223–253 (2004).
17. H. Möller, S. Grelier, P. Pardon, and V. Coma, Antimicrobial and physicochemical properties of chitosan-HPMC-based films. *J. Agric. Food. Chem.* **52**, 6585–6591 (2004).
18. R. Pantani, G. Gorrasi, G. Vigliotta, M. Murariu, and P. Dubois, PLA-ZnO nanocomposite films: Water vapor barrier properties and specific end-use characteristics. *Eur. Polym. J.* **49**, 3471–3482 (2013).
19. G. Findenig, S. Leimgruber, R. Kargl, S. Spirk, K. Stana-Kleinschek, and V. Ribitsch, Creating water vapor barrier coatings from hydrophilic components. *ACS Appl. Mat. Inter.* **4**, 3199–3206 (2012).
20. E. Fortunati, I. Armentano, A. Iannoni, M. Barbale, S. Zaccheo, M. Scavone, L. Visai, and J.M. Kenny, New multifunctional poly(lactide acid) composites: Mechanical, antibacterial, and degradation properties. *J. Appl. Polym. Sci.* **124**, 87–98 (2012).
21. M. Pluta, J.K. Jeszka, and G. Boiteux, Polylactide/montmorillonite nanocomposites: Structure, dielectric, viscoelastic and thermal properties. *Eur. Polym. J.* **43**, 2819–2835 (2007).
22. V. Peinado, L. García, Á. Fernández, and P. Castell, Novel lightweight foamed poly(lactic acid) reinforced with different loadings of functionalised Sepiolite. *Compos. Sci. Technol.* **101**, 17–23 (2014).
23. C. Chen, B.X. He, S.L. Wang, G.P. Yuan, and L. Zhang, Unexpected observation of highly thermostable transcrystallinity of poly(lactic acid) induced by aligned carbon nanotubes. *Eur. Polym. J.* **63**, 177–185 (2015).
24. N. Herrera, A.P. Mathew, and K. Oksman, Plasticized polylactic acid/cellulose nanocomposites prepared using melt-extrusion and liquid feeding: Mechanical, thermal and optical properties. *Compos. Sci. Technol.* **106**, 149–155 (2015).
25. X. Zhang and Y. Zhang, Reinforcement effect of poly(butylene succinate) (PBS)-grafted cellulose nanocrystal on toughened PBS/polylactic acid blends. *Carbohyd. Polym.* **140**, 374–382 (2016).
26. F. Luzi, E. Fortunati, A. Jiménez, D. Puglia, D. Pezzolla, G. Gigliotti, J.M. Kenny, A. Chiralt, and L. Torre, Production and characterization of PLA_PBS biodegradable blends reinforced with cellulose nanocrystals extracted from hemp fibres. *Ind. Crops Prod.* **93**, 276–289 (2016). DOI: org/10.1016/j.indcrop.2016.01.045.
27. W. Yang, F. Dominici, E. Fortunati, J.M. Kenny, and D. Puglia, Effect of lignin nanoparticles and masterbatch procedures on the final properties of glycidyl methacrylate-g-poly (lactic acid) films before and after accelerated UV weathering. *Ind. Crops Prod.* **77**, 833–844 (2015).
28. M. Grace, N. Chand, and S.K. Bajpai, Copper alginate-cotton cellulose (CACC) fibers with excellent antibacterial properties. *J. Eng. Fiber Fabr.* **4**, 1–14 (2009).

29. K. Shameli, M.B. Ahmad, W.M.Z.W. Yunus, N.A. Ibrahim, R.A. Rahman, M. Jokar, and M. Darroudi, Silver/poly(lactic acid) nanocomposites: preparation, characterization, and antibacterial activity. *Int. J. Nanomedicine* **5**, 573–579 (2010).
30. S. Therias, J.-F. Larché, P.-O. Bussière, J.-L. Gardette, M. Murariu, and P. Dubois, Photochemical behavior of polylactide/ZnO nanocomposite films. *Biomacromolecules* **13**, 3283–3291 (2012).
31. M. Matos Ruiz, J.Y. Cavaillé, A. Dufresne, J.F. Gérard, and C. Graillat, Processing and characterization of new thermoset nanocomposites based on cellulose whiskers. *Compos. Interfaces* **7**, 117–131 (2000).
32. M.A. Saïd Azizi Samir, F. Alloin, M. Paillet, and A. Dufresne, Tangling effect in fibrillated cellulose reinforced nanocomposites. *Macromolecules* **37**, 4313–4316 (2004).
33. Y.Q. Li, S.Y. Fu, and Y.W. Mai, Preparation and characterization of transparent ZnO/epoxy nanocomposites with high-UV shielding efficiency. *Polymer* **47**, 2127–2132 (2006).
34. S.C. Li and Y.N. Li, Mechanical and antibacterial properties of modified nano-ZnO/high-density polyethylene composite films with a low doped content of nano-ZnO. *J. Appl. Polym. Sci.* **116**, 2965–2969 (2010).
35. O. Yamamoto, Influence of particle size on the antibacterial activity of zinc oxide. *Int. J. Inorg. Mater.* **3**, 643–646 (2001).
36. Z.L. Wang, Zinc oxide nanostructures: Growth, properties and applications. *J. Phys.: Condens. Matter* **16**, R829–R858 (2004).
37. C. Riggio, V. Raffa, and A. Cuschieri, Synthesis, characterisation and dispersion of zinc oxide nanorods for biomedical applications. *IET Micro Nano Letters* **5**, 355–360 (2010).
38. Y. Liu, T. Morishima, T. Yatsui, T. Kawazoe, and M. Ohtsu, Size control of sol–gel-synthesized ZnO quantum dots using photo-induced desorption. *Nanotechnology* **22**, 215605 (2011).
39. Y. Liu, L. He, A. Mustapha, H. Li, Z.Q. Hu, and M. Lin, Antibacterial activities of zinc oxide nanoparticles against *Escherichia coli* O157:H7. *J. Appl. Microbiology* **107**, 1193–1201 (2009).
40. N. Jones, B. Ray, K.T. Ranjit, and A.C. Manna, Antibacterial activity of ZnO nanoparticle suspensions on a broad spectrum of microorganisms. *FEMS Microbiol. Lett.* **279**, 71–76 (2008).
41. K.T. Shalumon, K.H. Anulekha, S.V. Nair, S.V. Nair, K.P. Chennazhi, and R. Jayakumar, Sodium alginate/poly(vinyl alcohol)/nano ZnO composite nanofibers for antibacterial wound dressings. *Int. J. Biol. Macromol.* **49**, 247–254 (2011).
42. E. Fortunati, M. Peltzer, I. Armentano, L. Torre, A. Jimenez, and J.M. Kenny, Effects of modified cellulose nanocrystals on the barrier and migration properties of PLA nano-biocomposites. *Carbohyd. Polym.* **90**, 948–956 (2012).
43. F. Luzi, E. Fortunati, D. Puglia, R. Petrucci, J.M. Kenny, and L. Torre, Modulation of acid hydrolysis reaction time for the extraction of cellulose nanocrystals from *Posidonia oceanica* leaves. *J. Renew. Mater.* **4**, 190–198 (2016).
44. F. Bettaieb, R. Khiari, M. L., Hassan, M.N. Belgacem, J. Bras, A. Dufresne, and M.F. Mhenni, Preparation and characterization of new cellulose nanocrystals from marine biomass *Posidoniaoceanica*. *Ind. Crops Prod.* **72**, 175–182 (2015).
45. A. Mihranyan, Cellulose from cladophorales green algae: From environmental problem to high-tech composite materials. *J. Appl. Polym. Sci.* **119**, 2449–2460 (2011).
46. F. Bettaieb, R. Khiari, A. Dufresne, M.F. Mhenni, and M.N. Belgacem, Mechanical and thermal properties of Posidonia oceanica cellulose nanocrystal reinforced polymer. *Carbohyd. Polym.* 123, 99–104 (2015).
47. E. Fortunati, F. Luzi, D. Puglia, R. Petrucci, J.M. Kenny, and L. Torre, Processing of PLA nanocomposites with cellulose nanocrystals extracted from *Posidonia oceanica* waste: Innovative reuse of coastal plant. *Ind. Crops Prod.* **67**, 439–447 (2015).
48. F. Luzi, E. Fortunati, D. Puglia, R. Petrucci, J.M. Kenny, and L. Torre, Study of disintegrability in compost and enzymatic degradation of PLA and PLA nanocomposites reinforced with cellulose nanocrystals extracted from *Posidonia Oceanica*. *Polym. Degrad. Stab.* **121**, 105–115 (2015).
49. J. Jayaramudu, K. Das, M. Sonakshi, G.S.M. Reddy, B. Aderibigbe, R. Sadiku, and S.S. Ray, Structure and properties of highly toughened biodegradable polylactide/ZnO biocomposite films. *Int. J. Biol. Macromol.* **64**, 428–434 (2014).
50. L. Heux, G. Chauve, and C. Bonini, Nonflocculating and chiral-nematic self-ordering of cellulose microcrystals suspensions in nonpolar solvents. *Langmuir* **16**, 8210–8212 (2000).
51. E. Fortunati, I. Armentano, Q. Zhou, A. Iannoni, E. Saino, L. Visai, L.A. Berglund, and J.M. Kenny, Multifunctional bionanocomposite films of poly(lactic acid), cellulose nanocrystals and silver nanoparticles. *Carbohyd. Polym.* **87**, 1596–1605 (2012).
52. ASTM, Standard test method for specular gloss. Standard Designation: D523-89, in *Annual Book of American Society for Testing Materials*, ASTM, West Conshohocken, PA, USA (1999).
53. J. Turner, A. Riga, A. O'Connor, J. Zhang, and J. Collis, Characterization of drawn and undrawn poly-*L*-lactide films by differential scanning calorimetry. *J. Therm. Anal. Calorim.* **75**, 257–268 (2004).
54. ASTM, Standard test methods for water vapor transmission of materials. Standard Designations: E96–95, in *Annual Book of American Society for Testing Materials*, ASTM, West Conshohocken, PA, USA (1995).
55. M. Murariu, Y. Paint, O. Murariu, J.M. Raquez, L. Bonnaud, and P. Dubois, Current progress in the production of PLA–ZnO nanocomposites: Beneficial effects of chain extender addition on key properties. *J. Appl. Polym. Sci.* **132**, 42480–42491 (2015).
56. D. Bondeson, A. Mathew, and K. Oksman, Optimisation of the isolation of nanocrystals from microcrystalline cellulose by acid hydrolysis. *Cellulose* **13**, 171–180 (2006).
57. E. Fortunati, D. Puglia, M. Monti, L. Peponi, C. Santulli, J.M. Kenny, and L. Torre, Extraction of cellulose nanocrystals from *Phormium tenax* fibres. *J. Polym. Environ.* **21**, 319–328 (2013).

58. E. Fortunati, I. Armentano, A. Iannoni, and J.M. Kenny, Development and thermal behaviour of ternary PLA matrix composites. *Polym. Degrad. Stab.* **95**, 2200–2206 (2010).
59. E. Fortunati, F. Luzi, D. Puglia, A. Terenzi, M. Vercellino, L. Visai, C. Santulli, L. Torre, and J.M. Kenny, Ternary PVA nanocomposites containing cellulose nanocrystals from different sources and silver particles: Part II. *Carbohyd. Polym.* **97**, 837–848 (2013).
60. H. Abe, N. Takahashi, K.J. Kim, M. Mochizuki, and Y. Doi, Thermal degradation processes of end-capped poly(l-lactide)s in the presence and absence of residual zinc catalyst. *Biomacromolecules* **5**, 1606–1614 (2004).
61. J. Ahmed, Y.A. Arfat, E. Castro-Aguirre, and R. Auras, Thermal properties of ZnO and bimetallic Ag–Cu alloy reinforced poly(lactic acid) nanocomposite films. *J. Therm. Anal. Calorim.* **125**, 205–214 (2016).
62. M.P. Arrieta, E. Fortunati, F. Dominici, E. Rayon, J. Lopez, and J.M. Kenny, Multifunctional PLA–PHB/cellulose nanocrystal films: Processing, structural and thermal properties. *Carbohyd. Polym.* **107**, 16–24 (2014).
63. N. Bitinis, E. Fortunati, R. Verdejo, J. Bras, J. M. Kenny, L. Torre, and M.A. López-Manchado, Poly(lactic acid)/natural rubber/cellulose nanocrystal bionanocomposites. Part II: properties evaluation. *Carbohyd. Polym.* **96**, 621–627 (2013).
64. J.W. Rhim, H.M. Park, and C.S. Ha, Bio-nanocomposites for food packaging applications. *Prog. Polym. Sci.* **38**, 1629–1652 (2013).
65. A. Marra, C. Silvestre, D. Duraccio, and S. Cimmino, Polylactic acid/zinc oxide biocomposite films for food packaging application. *Int. J. Biol. Macromol.* **88**, 254–262 (2016).
66. Z. Yang, X. Zong, Z. Ye, B. Zhao, Q. Wang, and P. Wang, The application of complex multiple forklike ZnO nanostructures to rapid and ultrahigh sensitive hydrogen peroxide biosensors. *Biomaterials* **31**, 7534–7541 (2010).
67. G. Choudalakis and A.D. Gotsis, Permeability of polymer/clay nanocomposites: A review. *Eur. Polym. J.* **45**, 967–984 (2009).
68. K.R. Raghupathi, R.T. Koodali, and A.C. Manna, Size-dependent bacterial growth inhibition and mechanism of antibacterial activity of zinc oxide nanoparticles. *Langmuir* **27**, 4020–4028 (2011).
69. P.O. Bussiere, S. Therias, J.L. Gardette, M. Murariu, P. Dubois, and M. Baba, Effect of ZnO nanofillers treated with triethoxy caprylylsilane on the isothermal and non-isothermal crystallization of poly(lactic acid). *Phys. Chem. Chem. Phys.* **14**, 12301–12308 (2012).
70. J. Sawai and T. Yoshikawa, Quantitative evaluation of antifungal activity of metallic oxide powders (MgO, CaO and ZnO) by an indirect conductimetric assay. *J. Appl. Microbiol.* **96**, 803–809 (2004).